Disease progression and high field MRI in CADASIL

Liem, M.K.Y.

Chapter 8

7T MRI reveals diffuse iron deposition in the putamen and caudate nucleus in CADASIL

MK Liem, SAJ Lesnik Oberstein, MJ Versluis, MLC Maat-Schieman,
J Haan, AG Webb, MD Ferrari, MA van Buchem, J van der Grond

Submitted

ABSTRACT

Background and Purpose

Cerebral autosomal dominant arteriopathy with subcortical infarcts and leukoencephalopathy (CADASIL), a hereditary small vessel disease, is characterized by ischemic as well as neurodegenerative changes. Both of these brain processes have been linked to increased diffuse iron deposition in the brain. The aim of this study is to quantify diffuse iron deposition in CADASIL, using high-field in-vivo MRI and ex-vivo MRI imaging, as well as histopathologic analysis.

Methods

Twenty-five NOTCH3 mutation carriers and 15 healthy controls were examined using high resolution T2*-weighted imaging on a 7 Tesla whole body MRI scanner. Susceptibility weighted MRI scans were analyzed for areas of signal loss and increased phase shift. Phase shift measurements in deep grey nuclei, cortex and subcortical white matter were compared between mutation carriers and controls. For confirmation, ex-vivo brain specimens from another 3 CADASIL patients were analyzed for iron deposition using ex-vivo MRI combined with iron histochemistry.

Results

In-vivo MRI showed areas of decreased signal intensity and increased phase shift in mutation carriers. Compared to healthy controls, mutation carriers had significantly higher phase shift in the putamen ($p=0.0005$) and caudate nucleus ($p=0.008$). Ex-vivo MRI showed decreased signal intensity in the putamen and caudate nucleus in all specimens. Histochemistry confirmed the presence of iron deposition in these nuclei.

Conclusions

This study demonstrates increased diffuse iron accumulation in the putamen and caudate nucleus in CADASIL patients.

INTRODUCTION

Cerebral autosomal dominant arteriopathy with subcortical infarcts and leukoencephalopathy (CADASIL) is a hereditary small vessel disease caused by mutations in the *NOTCH3* gene.(1) The mutations cause abnormalities in small calibre arteries and arterioles of the cerebrum, consisting of deposition of granular osmiophilic material (GOM), degeneration of vascular smooth muscle cells and fibrous thickening of the vessel wall.(2)

Diffuse iron deposition in brain is a process that has been demonstrated in neurodegenerative diseases, in brain ischemia from large vessel occlusion, and in healthy subjects of older age.(3-7) Over the last few years, evidence is increasing that iron deposition is an important biomarker of various disease processes in the brain.(8;9) MRI scans in CADASIL, a small vessel disease, show both ischemic and secondary neurodegenerative changes.(10-12)

Increasingly sensitive detection of iron accumulation in the brain has been made possible by the advent of high field MRI, using magnitude and phase imaging of T2* gradient echo scans.(4;13)

The aim of this study is to investigate the potential presence and pattern of iron accumulation in CADASIL using high field MRI in vivo and ex vivo, as well as histopathological confirmation of iron accumulation.

METHODS

Patients

Participants consisted of 25 symptomatic (n=14) or asymptomatic (n=11) NOTCH3 mutation carriers (MCs) and 15 healthy age- and sex-matched volunteers. Informed consent was obtained from all participants. Approval for the study was given by the medical ethics committee of the Leiden University Medical Center.

A full medical history was obtained. Disease duration was determined based on first occurrence of neurological symptoms excluding migraine aura.

In-vivo Magnetic Resonance Imaging

MRI was performed on a whole body human 7T MR system (Philips Healthcare, Best, the Netherlands). Whole brain imaging was performed with all sequences in an axial plane parallel to the inferior border of the genu and splenium of the corpus callosum. Additionally, high resolution imaging in a 2.2 cm thick axial slab of interest that included the thalamus, corpus striatum and parts of the frontal, parietal, temporal as well as occipital lobes was performed.

The following scan protocol was used:

- Whole brain 3D T1-weighted images with a scan duration of 12 minutes; repetition time (TR)/ echo time (TE)/ flip angle = 19 ms / 9.2 ms / 8°, 280 slices, 210 x 169 mm field of view, 700 x 563 matrix size - resulting in a nominal resolution of 0.3 x 0.3 x 0.5 mm.
- Whole brain 3D T2*-weighted gradient echo images with a scan duration of 5:46 minutes; TR/TE/FA = 24 ms / 15 ms / 15°, 280 slices, 220 x 182 mm field of view, 368 x 303 matrix size - resulting in a nominal resolution of 0.6 x 0.6 x 0.5 mm.
- Whole brain 2D T2-weighted turbo spin echo images with a scan duration of 6:04 minutes; TR/TE/FA = 14000 ms / 105 ms / 90°, slice thickness 3.0 mm with a 0.3 mm interslice gap, 40 slices, 230 x 182 mm field of view, 384 x 288 matrix size - resulting in a nominal resolution of 0.6 x 0.6 x 3.0 mm
- Slice-of-interest high resolution imaging: 2D T2*-weighted gradient echo images with a scan duration of 9:25 minutes; TR/TE/FA = 720ms / 21 ms / 45°, slice thickness 1.0 mm with a 0.1 mm interslice gap, 20 slices, 240 x 180 mm field of view, 1000 x 750 matrix size - resulting in a nominal resolution of 0.24 x 0.24 x 1.0 mm (adapted from Duyn and coworkers(14)). The phase images were subsequently unwrapped by highpass filtering with a 92x92 kernel size.(15)
- Slice-of-interest high resolution imaging: 2D T2-weighted turbo spin echo images with a scan duration of 9:09 minutes; TR/TE/FA = 3000 ms / 58 ms / 110°, slice thickness 1.0 mm with a 0.1 mm interslice gap, 20 slices, 240 x 180 mm field of view, 480/360 matrix size - resulting in a nominal resolution of 0.5 x 0.5 x 1.0 mm.

MRI Analysis

Before analyzing diffuse iron deposition, the magnitude images of the T2*-weighted scans were first inspected for the possible presence of microbleeds since they may interfere with measurements of diffuse iron deposition. Analysis was done by an observer who was blinded to patient data.

Microbleeds were defined as focal areas of signal loss on the whole brain T2*-weighted images with a round or ovoid shape, that did not appear in successive slices, showed a blooming effect on T2*-weighted images and that were devoid of signal hyperintensity on T1- or T2-weighted spin-echo images.(16) The number and location of focal areas of signal loss were counted on a digital workstation.

To analyze diffuse iron accumulation, we first inspected the magnitude images of the T2*-weighted images visually for diffuse areas of signal loss. Diffuse hypointensities in the basal ganglia and thalamus were assessed using a subjective two-point scale, and were scored as being present or absent.

To further quantify the amount of diffuse iron accumulation, we used the unwrapped phase images, since they provide a measure of iron content that is relatively independent of other tissue characteristics, such as gliosis, water content, etc.(4) We measured mean phase shift on the unwrapped phase images of the high-resolution multi slice T2*-weighted gradient scans after manually outlining regions of interest (ROIs) bilaterally in the globus pallidus, putamen, head of caudate nucleus, thalamus and in the cortex and subcortical white matter of the frontal, temporal, parietal and occipital lobes. Focal areas of phase shift, attributable to cerebral microbleeds or areas of calcifications, were excluded from the ROIs. ROIs in deep grey nuclei were drawn on the slice that best visualized the structure and followed the shape of the structure. ROIs in cortical grey matter and subcortical white matter were drawn on 5 different slices, each 4 mm apart, and consisted of 5 randomly distributed circular ROIs per lobe per slice in the cortex and 1 circular ROI per lobe per slice in the subcortical white matter. Mean phase shift in all ROIs was measured on a digital workstation.

Postmortem MRI examinations

Formalin-fixed, approximately 10-mm-thick, coronal hemispheric brain slices from another 3 CADASIL patients (patient 1: female, 58 years old; patient 2: male, 64 years old; patient 3: female, 60 years old) were investigated, which included the basal ganglia and thalamus (n=2), white matter (n=3) and cortex (n=3). Fixation duration ranged from 8 – 11 years. In all cases, informed consent was obtained from the patient or family to perform autopsy and to use the tissues for research purposes. The diagnosis was genetically confirmed and neuropathologic findings in these patients were consistent with the diagnosis of CADASIL.

The brain specimen was placed between two perspex plates (170 mm long, 80 mm broad) adjusted to the thickness of the brain slice. Ten holes per plate of 25 mm in diameter were made to allow air bubbles to escape. The brain specimen between the plates was positioned in a plastic container filled with formalin and shaken by hand to remove air bubbles. The container was fixed in the head coil using cushions. MRI was performed with the same whole body human 7T MR system.

The following scan protocol was used (adapted from van Rooden and coworkers(17)):

- High resolution 0.18 x 0.18 x 0.18 mm 3D T2*-weighted gradient echo images with a scan duration of 6 hours and 42 minutes (number of sample averages (NSA)=12); TR/TE/FA = 60ms / 25 ms / 10°, slice thickness 0.18 mm, 62 slices, 180 x 99 mm field of view, 1000 x 552 matrix size - resulting in a nominal resolution of 0.18 x 0.18 x 0.18 mm.
- High resolution 0.18 x 0.18 x 0.18 mm 3D T1-weighted gradient echo images with a scan duration of 14 hours and 5 minutes (NSA=32); TR/TE/FA = 30ms / 4.9ms / 50°, slice thickness 0.18 mm, 61 slices, 180 x 99 mm field of view, 1000x552 matrix size - resulting in a nominal resolution of 0.18 x 0.18 x 0.18 mm.

- High resolution 0.3 x 0.3 x 0.3 mm 3D T2-weighted spin echo images with a scan duration of 9 hours and 32 minutes (NSA=2); TR/TE/FA 1000 ms / 50 ms / 90°, slice thickness 0.3 mm, 37 slices, 180 x 99 mm field of view, 600x333 matrix size - resulting in a nominal resolution of 0.3 x 0.3 x 0.3 mm.

Because of the small number of post-mortem scans available, we analyzed the scans by visual inspection of areas of signal loss in cortex and deep gray nuclei on magnitude images, rather than performing quantitative phase shift analysis. Analysis was performed on a digital workstation.

Histopathologic analysis

After imaging, the brain slices were embedded in paraffin and cut into 10-µm-thick sections. Sections were stained with hematoxylin and eosin or Luxol fast blue for routine histopathological examination. Perl's staining was used to identify iron and von Kossa's staining was used to identify calcium. Location and pattern of iron deposition and calcium deposits were recorded. Differences in staining severity were assessed qualitatively.

Statistics

Statistical analysis was performed using the SPSS-16 statistical software package (SPSS Inc., Chicago, IL). Differences in age and sex between *NOTCH3* MCs and controls were analyzed using Student's t-tests and chi square tests. Differences in prevalence of diffuse hypointensities in cortex, white matter and deep grey nuclei in MCs and controls were analyzed using Fisher's exact test. Differences in mean phase shift between MCs and controls, and between symptomatic MCs and asymptomatic MCs, were compared using analysis of covariance (ANCOVA), with age as a covariate to correct for possible age differences. Significance thresholds were set at $p < 0.01$ in order to correct for multiple testing. Mean phase shifts were additionally correlated with age using the Pearson correlation coefficient.

RESULTS

Age and sex distribution of MCs (12 males and 13 females; mean age: 46.5 years, SD: 12.2) and controls (9 males and 6 females; mean age: 44.7 years, SD: 12.2) were comparable. The average disease duration of the 14 symptomatic MCs was 7.7 years (range 1 to 21 years).

In vivo MRI

Focal areas of signal loss on magnitude images

Eleven MCs (44%) had microbleeds, mostly (69%) in the thalamus, but also in the basal ganglia (9%), subcortical white matter (8%), infratentorium (7%), cortex (4%) and deep white matter (3%). The number of microbleeds per patient ranged from 1 - 27 (mean 6.8).

Diffuse areas of signal loss on magnitude images

Compared to controls, the MCs had a higher prevalence of diffuse areas of signal loss in the putamen (15/25 MCs, 3/12 controls, p = 0.02) and caudate nucleus (11/25 MCs, 1/15 nonMCs, p=0.02). The prevalence of diffuse areas of signal loss did not differ between MCs and nonMCs in the globus pallidus (13/25 MCs, 7/15 controls, p=1.00) and thalamus (2/25 MCs, 0/15 controls, p=0.51). No diffuse areas of signal loss were identified in the white matter or cortex of MCs or controls.

The prevalence of diffuse areas of signal loss was higher in symptomatic MCs than in asymptomatic MCs in the putamen (10/14 symptomatic MCs and 5/11 asymptomatic MCs) and caudate nucleus (7/14 symptomatic MCs and 4/11 asymptomatic MCs). However, these differences were not statistically significant ($p > 0.05$).

Analysis of phase shift on phase images

MCs demonstrated a symmetrically (Pearson correlation coefficient greater than 0.8) increased phase shift compared to controls in the putamen ($p = 0.0005$) and caudate nucleus ($p = 0.008$) (table 1, figure 1 and figure 2). The amount of phase shift in the globus pallidus and thalamus, and in the cortex and subcortical white matter did not differ between MCs and controls (table 1).

Symptomatic MCs had higher mean phase shift values in the putamen and caudate nucleus than asymptomatic MCs (symptomatic: putamen = 0.490 rad, caudate nucleus = 0.179 rad; asymptomatic: putamen = 0.361 rad, caudate nucleus = 0.149 rad). However, these differences were not statistically significant. Similarly, no significant differences in phase shift were found between symptomatic and asymptomatic MCs in the globus pallidus, thalamus, cortex and subcortical white matter.

In MCs an increased phase shift in the putamen and caudate nucleus was associated with higher age (putamen: $B = 0.008$ rad per year, $r = 0.47$, $p = 0.02$; caudate nucleus: $B = 0.003$ rad per year, $r = 0.45$, $p = 0.02$). In the healthy controls, no association was found between age and phase shift in putamen and caudate nucleus.

Table 1. Mean phase shift in deep gray nuclei, cortex and white matter

	CADASIL (n = 25)	Control (n = 15)	P value*
Deep gray nuclei			
Globus Pallidus (mean,SD)	0.271 (0.098)	0.261 (0.115)	n.s.
Putamen (mean,SD)	0.434 (0.204)	0.204 (0.082)	0.0005
Caudate nucleus (mean,SD)	0.166 (0.081)	0.100 (0.047)	0.008
Thalamus (mean,SD)	0.034 (0.036)	0.021 (0.030)	n.s.
Cortex			
Frontal	0.157 (0.034)	0.155 (0.028)	n.s.
Parietal	0.178 (0.032)	0.185 (0.025)	n.s.
Temporal	0.211 (0.040)	0.215 (0.025)	n.s.
Occipital	0.206 (0.038)	0.213 (0.020)	n.s.
White Matter			
Frontal	-0.119 (0.019)	-0.121 (0.023)	n.s.
Parietal	-0.131 (0.028)	-0.137 (0.022)	n.s.
Temporal	-0.130 (0.022)	-0.132 (0.022)	n.s.
Occipital	-0.153 (0.025)	-0.163 (0.035)	n.s.

Mean phase shift values expressed in rad

n.s. = not significant using a significance threshold of p = 0.01 in order to correct for multiple comparisons

Figure 1. T2*-weighted gradient echo scans: magnitude images (top row) and unwrapped phase images (bottom row) of an approximately 60 years old† CADASIL patient (left) and an approximately 60 years† control subject (right), showing increased signal loss and phase shift in the putamen and caudate nucleus of the CADASIL patient.

† = exact age not disclosed for patient privacy reasons

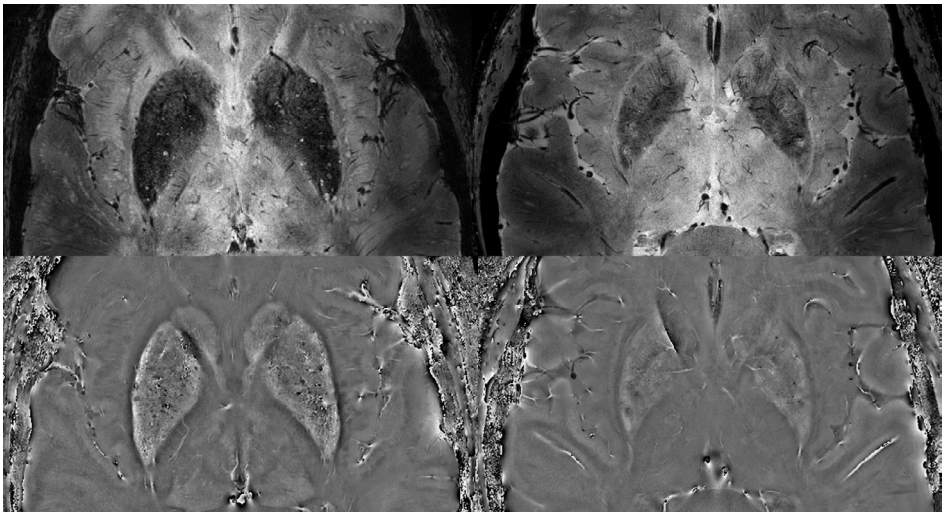

Figure 2: Phase shift in putamen and caudate nucleus in MCs and controls

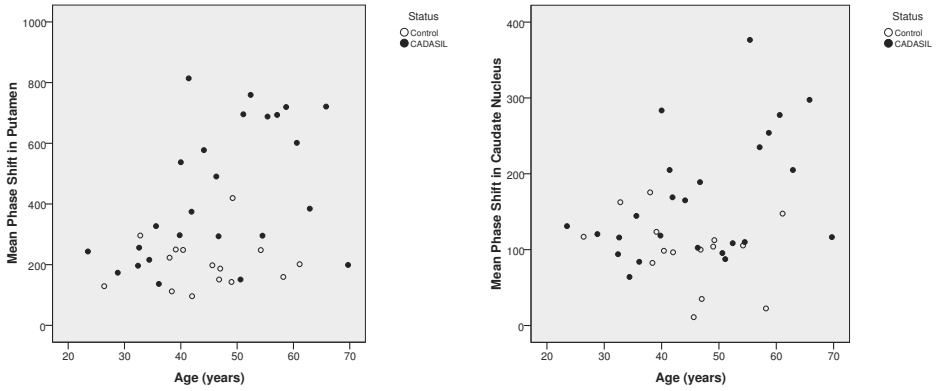

Post-mortem MRI and histopathologic analysis

Visual inspection of the post-mortem MRI scans revealed marked diffuse signal loss in the putamen and caudate nucleus and to a lesser extent in the globus pallidus of the brain specimens (figure 3).

Figure 3. MRI and histopathological iron staining of post-mortem brain tissue of a CADASIL patient. Left: T2*-weighted gradient echo MRI scan showing signal loss in the putamen (solid arrows) and caudate nucleus (dashed arrows). Middle: Iron staining of the same slice shows iron staining in the putamen and caudate nucleus. Right: detail of the iron stain from the the putamen (40 x magnification) shows iron deposition in a perivascular and diffuse distribution.

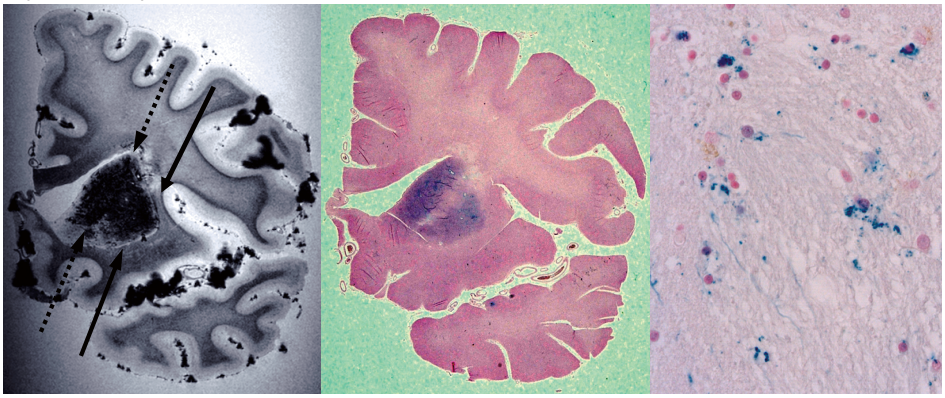

Iron histochemistry of the brain specimens revealed macroscopic evidence of iron deposition in the caudate nucleus and putamen and to a lesser extent in the globus pallidus. The pattern of iron staining matched the pattern of signal loss visible on post-mortem MRI (figure 3). No iron staining was observed macroscopically in the cerebral cortex (except for a remnant of a hemorrhage in the temporal cortex of 1 patient), the subcortical white matter or the thalamus.

Microscopy showed that the iron deposits in the caudate nucleus and putamen were located scattered throughout the parenchyma as well as perivascularly, and that they were mostly associated with cells with morphology of glia. Microscopy also showed mild diffuse staining of myelin in the subcortical white matter, with delicate patches of cell-associated iron deposits. No microscopic iron deposits were found in the thalamus and in the cortex.

Von Kossa staining revealed sporadic calcium deposits in the globus pallidus, putamen and caudate nucleus. This calcium staining was mild and did not match the pattern of MRI hypointensities.

DISCUSSION

This combined MRI and histopathological study shows that CADASIL patients have diffuse areas of increased hypointensity and phase shift in the putamen and caudate nucleus, which we show to be caused by progressive local iron accumulation.

Increased iron accumulation has not been demonstrated before in CADASIL or in other forms of small vessel disease, but has mainly been associated with neurodegenerative diseases such as Alzheimer's and Huntington disease and with large vessel stroke.(3;4;6;7) Iron accumulation is believed to be associated with progression of neurodegenerative diseases, but the mechanism is still unknown.(18) Possibly, in CADASIL ischemic damage to the brain causes a disturbance in iron metabolism and homeostasis resulting in a release of iron from its protein carriers.(5;19)

Although ischemic damage and secondary neurodegeneration in CADASIL affects all brain regions, including white matter and cerebral cortex,(20) the iron deposition we found was limited to the striatum. This pattern is more compatible with iron deposition in aging and in degenerative diseases, than with iron deposition in large vessel stroke.(3;4;6;21) A possible explanation for this distribution is that when brain ischemia leads to a release of iron molecules in the cortex and white matter, this iron may be taken up by neuronal dendrites and be transported along neuronal axons to their sites of projection, the deep grey nuclei, where the iron is released and stored in oligodendroglial cells.(7) Since ischemic brain damage in small vessel disease is considered to be more chronic than in large vessel stroke,(22) this mechanism to remove the iron from the cortex and white matter may work more efficiently.

An alternative explanation for the distribution of iron in the striatum is that the deposition of iron molecules is not a direct result of brain ischemia, but rather a consequence of the secondary neurodegeneration. Possibly, the demyelination of white matter tracts and the

atrophy of cerebral cortex lead to a decreased demand of iron from the storage place in the deep gray nuclei, causing a chronic accumulation of iron in the striatum.(7)

The effects of the increased iron levels in deep brain nuclei in this study population are unknown. In general, increased brain iron levels may lead to cerebral damage by interfering with protein synthesis or by increasing the vulnerability to oxidative stress.(23;24) In CADASIL, this may lead to worsening of clinical symptoms and to faster clinical disease progression. In our study the symptomatic CADASIL patients did indeed have higher values of phase shift than the asymptomatic MCs, which suggests that iron deposition is associated with disease severity. However, since these differences were not statistically significant, it remains unclear whether this association is true. Studies with a larger sample size need to be performed to confirm the relation between iron deposition and clinical disease severity in CADASIL. Eventually, the present findings could open new venues to modify the course of the disease in CADASIL, for example by using iron chelators or inhibitors of oxidative stress.

We measured iron deposition indirectly by detecting signal loss on magnitude images and measuring increased phase shift on phase images, and not by direct measurement of iron concentration which is still an area of contention in terms of quantitation using MRI. Causes of decreased signal intensity other than iron, such as calcifications or depositions of other types of metal cannot be ruled out on the MRI scans. However, histopathologic analysis showed that the pattern of hypointensity observed on MRI matches the pattern of iron staining on histochemistry.

In conclusion, high field MR imaging demonstrates progressive diffuse areas of T2* hypointensity and phase shift in the striatum in CADASIL, indicating that progressive iron deposition is associated with the pathology of CADASIL, and possibly of other small vessel diseases. Further research is needed to elucidate the underlying pathophysiology and possible implications.

REFERENCE LIST

(1) Joutel A, Vahedi K, Corpechot C, Troesch A, Chabriat H, Vayssiere C, et al. Strong clustering and stereotyped nature of Notch3 mutations in CADASIL patients [see comments]. Lancet 1997; 350(9090):1511-5.

(2) Ruchoux MM, Guerouaou D, Vandenhaute B, Pruvo JP, Vermersch P, Leys D. Systemic vascular smooth muscle cell impairment in cerebral autosomal dominant arteriopathy with subcortical infarcts and leukoencephalopathy. Acta Neuropathol (Berl) 1995;89(6):500-12.

(3) Bartzokis G, Cummings J, Perlman S, Hance DB, Mintz J. Increased basal ganglia iron levels in Huntington disease. Arch Neurol 1999 May;56(5):569-74.

(4) Zhu WZ, Zhong WD, Wang W, Zhan CJ, Wang CY, Qi JP, et al. Quantitative MR phase-corrected imaging to investigate increased brain iron deposition of patients with Alzheimer disease. Radiology 2009 Nov;253(2):497-504.

(5) Lipscomb DC, Gorman LG, Traystman RJ, Hurn PD. Low molecular weight iron in cerebral ischemic acidosis in vivo. Stroke 1998 Feb;29(2):487-92.

(6) Cross PA, Atlas SW, Grossman RI. MR evaluation of brain iron in children with cerebral infarction. AJNR Am J Neuroradiol 1990 Mar;11(2):341-8.

(7) Dietrich RB, Bradley WG, Jr. Iron accumulation in the basal ganglia following severe ischemic-anoxic insults in children. Radiology 1988 Jul;168(1):203-6.

(8) Penke L, Valdes Hernandez MC, Maniega SM, Gow AJ, Murray C, Starr JM, et al. Brain iron deposits are associated with general cognitive ability and cognitive aging. Neurobiol Aging 2010 Jun 7.

(9) Salvador GA, Uranga RM, Giusto NM. Iron and mechanisms of neurotoxicity. Int J Alzheimers Dis 2010;2011:720658.

(10) van den Boom R, Lesnik Oberstein SA, Ferrari MD, Haan J, Van Buchem MA. Cerebral autosomal dominant arteriopathy with subcortical infarcts and leukoencephalopathy: MR imaging findings at different ages--3rd-6th decades. Radiology 2003 Dec;229(3):683-90.

(11) O'Sullivan M, Ngo E, Viswanathan A, Jouvent E, Gschwendtner A, Saemann PG, et al. Hippocampal volume is an independent predictor of cognitive performance in CADASIL. Neurobiol Aging 2009 Jun;30(6):890-7.

(12) Chowdhury MH, Nagai A, Bokura H, Nakamura E, Kobayashi S, Yamaguchi S. Age-Related Changes in White Matter Lesions, Hippocampal Atrophy, and Cerebral Microbleeds in Healthy Subjects Without Major Cerebrovascular Risk Factors. J Stroke Cerebrovasc Dis 2010 Jul 14.

(13) Yao B, Li TQ, Gelderen P, Shmueli K, de Zwart JA, Duyn JH. Susceptibility contrast in high field MRI of human brain as a function of tissue iron content. Neuroimage 2009 Feb 15;44(4):1259-66.

(14) Duyn JH, van Gelderen P, Li TQ, de Zwart JA, Koretsky AP, Fukunaga M. High-field MRI of brain cortical substructure based on signal phase. Proc Natl Acad Sci U S A 2007 Jul 10;104(28):11796-801.

(15) Haacke EM, Xu Y, Cheng YC, Reichenbach JR. Susceptibility weighted imaging (SWI). Magn Reson Med 2004 Sep;52(3):612-8.

(16) Greenberg SM, Vernooij MW, Cordonnier C, Viswanathan A, Al-Shahi SR, Warach S, et al. Cerebral microbleeds: a guide to detection and interpretation. Lancet Neurol 2009 Feb;8(2):165-74.

(17) Van Rooden S, Maat-Schieman ML, Nabuurs RJ, Van der Weerd L, Van Duijn S, Van Duinen SG, et al. Cerebral Amyloidosis: Postmortem Detection with Human 7.0-T MR Imaging System. Radiology 2009 Sep 29;253:788-96.

(18) Berg D, Youdim MB. Role of iron in neurodegenerative disorders. Top Magn Reson Imaging 2006 Feb;17(1):5-17.

(19) Selim MH, Ratan RR. The role of iron neurotoxicity in ischemic stroke. Ageing Res Rev 2004 Jul; 3(3):345-53.

(20) Jouvent E, Mangin JF, Porcher R, Viswanathan A, O'Sullivan M, Guichard JP, et al. Cortical changes in cerebral small vessel diseases: a 3D MRI study of cortical morphology in CADASIL. Brain 2008 Aug;131(Pt 8):2201-8.

(21) Milton WJ, Atlas SW, Lexa FJ, Mozley PD, Gur RE. Deep gray matter hypointensity patterns with aging in healthy adults: MR imaging at 1.5 T. Radiology 1991 Dec;181(3):715-9.

(22) Pantoni L, Garcia JHa. The significance of cerebral white matter abnormalities 100 years after Binswanger's report. A review. Stroke 1995;26(7):1293-301.

(23) Gutteridge JM. Iron and oxygen radicals in brain. Ann Neurol 1992;32 Suppl:S16-S21.

(24) Gaasch JA, Lockman PR, Geldenhuys WJ, Allen DD, Van der Schyf CJ. Brain iron toxicity: differential responses of astrocytes, neurons, and endothelial cells. Neurochem Res 2007 Jul;32(7):1196-208.